

THE MASS-METALLICITY RELATION OF GLOBULAR CLUSTERS IN THE CONTEXT OF NONLINEAR COLOR-METALLICITY RELATIONS

JOHN P. BLAKESLEE¹, MICHELE CANTIELLO², AND ERIC W. PENG^{3,4}

To Appear in ApJ, Vol. 710, February 2010

ABSTRACT

Two recent empirical developments in the study of extragalactic globular cluster (GC) populations are the color–magnitude relation of the blue GCs (the “blue tilt”) and the nonlinearity of the dependence of optical GC colors on metallicity. The color–magnitude relation, interpreted as a mass–metallicity relation, is thought to be a consequence of self-enrichment. Nonlinear color–metallicity relations have been shown to produce bimodal color distributions from unimodal metallicity distributions. We simulate GC populations including both a mass–metallicity scaling relation and nonlinear color–metallicity relations motivated by theory and observations. Depending on the assumed range of metallicities and the width of the GC luminosity function (GCLF), we find that the simulated populations can have bimodal color distributions with a “blue tilt” similar to observations, even though the metallicity distribution appears unimodal. The models that produce these features have the relatively high mean GC metallicities and nearly equal blue and red peaks characteristic of giant elliptical galaxies. The blue tilt is less apparent in the models with metallicities typical of dwarf ellipticals; the narrower GCLF in these galaxies has an even bigger effect in reducing the significance of their color–magnitude slopes. We critically examine the evidence for nonlinearity versus bimodal metallicities as explanations for the characteristic double-peaked color histograms of giant ellipticals and conclude that the question remains open. We discuss the prospects for further theoretical and observational progress in constraining the models presented here and for uncovering the true metallicity distributions of extragalactic globular cluster systems.

Subject headings: galaxies: elliptical and lenticular, cD — galaxies: fundamental parameters — galaxies: star clusters — globular clusters: general

1. INTRODUCTION

Massive early-type galaxies have globular cluster (GC) systems that follow bimodal color distributions (e.g., Gebhardt & Kissler-Patig 1999; Larsen et al. 2001; Harris et al. 2006; Peng et al. 2006, hereafter P06). Before this was a commonly recognized feature of such systems, Ashman & Zepf (1992) discussed the possibility of GC color bimodality based on the simple idea that ellipticals are the remnants of dissipationally merged pairs of spirals (e.g., Toomre 1977). In this picture, a merger-formed population of red, relatively high-metallicity GCs would then appear distinct from the blue, metal-poor GCs of the progenitor spirals.

The actual formation histories of ellipticals appear to have been more complex (see for example the review by Renzini 2006). In particular, most of the stars in large ellipticals today are believed to have formed early, in a series of rapid starbursts at redshifts $z > 2$, whereas the hierarchical assembly of these galaxies continued to $z < 1$ through “dry” (dissipationless) mergers (e.g., De Lucia et al. 2006; Menci et al. 2008; Kodama et al. 2007; Thomas et al. 2005). Such hierarchical formation models do not naturally produce bimodal GC metallicity distributions in most elliptical galaxies (Beasley et al. 2002; Kravtsov & Gnedin 2005). Instead, the stochastic nature of the formation would be expected to result in approximately Gaussian distributions. Thus, while some galaxies with quiet histories like the Milky Way’s may have bimodal

GC metallicity distributions if they formed their stars in just a few discrete bursts, it is difficult to see how bimodality would be nearly universal in this context.

An alternative model was put forth by Côté et al. (1998) in which ellipticals *form* with unimodal, relatively rich GC metallicity distributions and later acquire the blue GC component through dissipationless mergers with early-type dwarfs. This explanation appears more consistent with hierarchical formation models. However, the universality of the bimodality, even at intermediate luminosities, and the asymmetric tail of red GCs in dwarf ellipticals, would again be surprising in this scenario.

Models of GC color distributions have typically assumed linear conversions between metallicity and optical colors. The observed color bimodality thereby became equated with bimodality in metallicity. In contrast, P06 showed that the empirical transformation from metallicity to the broad-baseline ($g-z$) color is distinctly nonlinear. An earlier indication of such nonlinearity for the ($C-T_1$) color index (Harris & Harris 2002; Cohen et al. 2003) has also been confirmed (Lee et al. 2008). Further, Yoon et al. (2006) pointed out that nonlinear color–metallicity relations predicted by their simple stellar population (SSP) models naturally produce bimodal color histograms from unimodal metallicity distributions. Such nonlinearities are commonly predicted by realistic SSP models that try to reproduce the structure in stellar color–magnitude diagrams as a function of metallicity (see Cantiello & Blakeslee 2007, hereafter CB07). This provides an alternative, simple explanation for the near-universality of bimodal GC color distributions, although the idea remains controversial as we discuss in Sec. 4 below.

It is not surprising that as observations and models improve, deviations from the simplest linear assumptions become im-

¹ Herzberg Institute of Astrophysics, National Research Council of Canada, Victoria, BC V9E 2E7, Canada; John.Blakeslee@nrc.ca

² INAF-Osservatorio Astronomico di Teramo, via M. Maggini, I-64100, Teramo, Italy

³ Department of Astronomy, Peking University, Beijing 100871, China

⁴ Kavli Institute for Astronomy and Astrophysics, Beijing 100871, China

portant. A related example is the dependence of galaxy surface brightness fluctuation magnitudes on integrated color: linear fits sufficed at the level of accuracy of ground-based data, but the latest *HST* studies (Mei et al. 2007; Blakeslee et al. 2009) clearly show a wavy relation reminiscent of that between metallicity and color. Galaxy scaling relations are another example where nonlinearity has become evident amid the continuity of structural properties in new samples of galaxies spanning many orders of magnitude (Côté et al. 2008). Even the Cepheid period-luminosity relation has been found to exhibit significant nonlinearity (Ngeow et al. 2009). Although the errors in derived quantities (e.g., distance modulus or metallicity) resulting from such nonlinearities are often small for individual objects, the implications for the distributions of these quantities derived for large populations can be profound.

Another development has been the discovery that GCs in the blue peak of the color distribution tend to be redder at brighter magnitudes (Harris et al. 2006; Mieske et al. 2006; Strader et al. 2006). Dubbed “the blue tilt,” the effect is subtle, but further evidence confirms it is real (Harris 2009; Peng et al. 2009). The likely explanation is that the most massive GCs were able to self-enrich to a small extent, thus producing a mass-metallicity relation (e.g., Dopita & Smith 1986; Morgan & Lake 1989; Brown et al. 1991; Recchi & Danziger 2005; Strader & Smith 2008; Bailin & Harris 2009). The tendency is much less obvious for the red-peak GCs, despite the otherwise lockstep behavior of the two peaks, which is strong evidence that they formed under similar conditions (P06; Larsen et al. 2001). However, the red peak is broader because of the nonlinear color-metallicity relation, and it usually does not reach as high in optical luminosity, at least partly because of the decrease in luminosity-to-mass ratio with increasing metallicity. A weak “red tilt” is expected theoretically (Bailin & Harris 2009), and there is evidence for this in some cases (Mieske et al. 2006; Lee et al. 2008).

The purpose of this work is to bring together these two recent developments in the study of extragalactic GC systems: we explore the nature of the blue tilt in the context of unimodal metallicity distributions with nonlinear dependence of color on metallicity. To do this, we assume a mass-metallicity relation consistent with the findings of recent studies. The following section describes our approach in more detail, and Sec. 3 presents the consequences for the observed blue tilt under various assumptions about the range of GC metallicities and luminosities. The implications of our results and the question of bimodality are considered in Sec. 4. The final section summarizes our conclusions.

2. METHOD

Our goal is to investigate the presence and significance of the “blue tilt” — the color-magnitude relation of the blue peak GCs — in the case of unimodal metallicity distributions following an empirically motivated mass-metallicity relation (MMR) and the nonlinear color-metallicity relations both observed and predicted by detailed SSP modeling. We also examine the “tilt” of the red peak GCs in this scenario. For the sake of generality in this initial investigation, we try to keep our assumptions as simple as possible while still being realistic enough to yield useful insights.

2.1. Color–Metallicity Relations

P06 presented an empirical $[\text{Fe}/\text{H}]$ –($g-z$) relation based on their photometry and spectroscopic metallicities for a com-

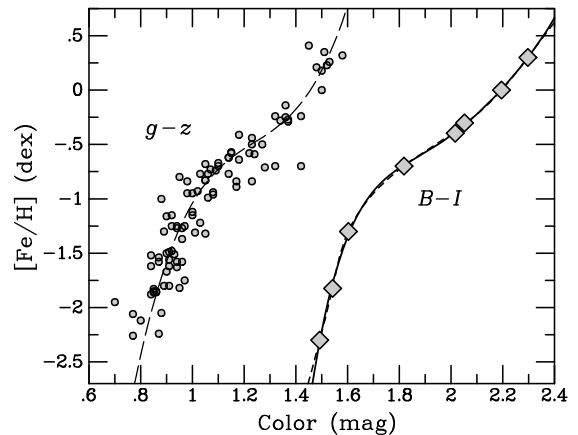


FIG. 1.— Empirical ($g-z$) and model ($B-I$) color-metallicity relations. The circles show data for Milky Way and Virgo cluster GCs (Peng et al. 2006), and the long-dashed curve is a fourth-order polynomial fit to the data. The diamonds show predictions for ($B-I$) from the 13 Gyr Teramo SPoT models used in this study. The solid curve is a fifth-order polynomial fit, while the short-dashed curve is a cubic spline interpolation/extrapolation of the models. As commonly used for these indices, the ($B-I$) colors are on the Vega-based Johnson-Cousins system while ($g-z$) is given in AB magnitudes. The conversion from the AB to Vega system for ($g-z$) is +0.64 mag; thus, these color indices are quite similar, but the data have a steeper slope than the models at the red end.

bination of 95 Milky Way, M49 (NGC 4472), and M87 GCs (see their Fig. 11). The Milky Way GC data are part of a larger project to produce a homogeneous database of integrated colors for the entire Galactic GC system in the SDSS photometric bandpasses (West et al. 2006; M. West et al., in preparation). The inclusion of the Virgo galaxy GC metallicities from Cohen et al. (1998, 2003) was necessary to characterize the relation at high metallicity. This adds uncertainty because the conversion from the Lick indices to the Zinn & West (1984) metallicity scale is not well calibrated above solar metallicity and involves some extrapolation (see Fig. 14 of Cohen et al. 1998). However, the extrapolation is strictly linear and extends $\lesssim 0.5$ dex at the metal-rich end, so it could not introduce a nonlinearity in the $[\text{Fe}/\text{H}]$ –($g-z$) relation. Intrinsic trends in age and/or alpha-enhancement with metallicity could potentially introduce biases in the metallicity scale (see the discussion in P06), but such trends would not change our results if they involve a simple scaling factor. Since we wish to avoid ad hoc assumptions about model ages and abundance ratios as far as possible, we prefer to adopt empirical calibrations in our analysis, and this remains the best empirically-based color-metallicity relation available.

For simplicity, P06 used a broken linear fit to the curved $[\text{Fe}/\text{H}]$ –($g-z$) relation, excluding the highest metallicity GCs which would have required additional curvature. To better characterize the full data set presented in P06, we fit a quartic polynomial using robust orthogonal regression (GaussFit; Jefferys et al. 1988) and find the following relation

$$[\text{Fe}/\text{H}] = -33.74 + 79.81(g-z) - 66.69(g-z)^2 + 20.66(g-z)^3 - 1.08(g-z)^4, \quad (1)$$

which we plot in Figure 1 along with the data points from P06. Note that the empirical ($g-z$) colors are calibrated to the AB system, and the conversion from AB to Vega-based magnitudes for ($g-z$) is +0.64 mag.

Other color indices used in recent studies of GC color dis-

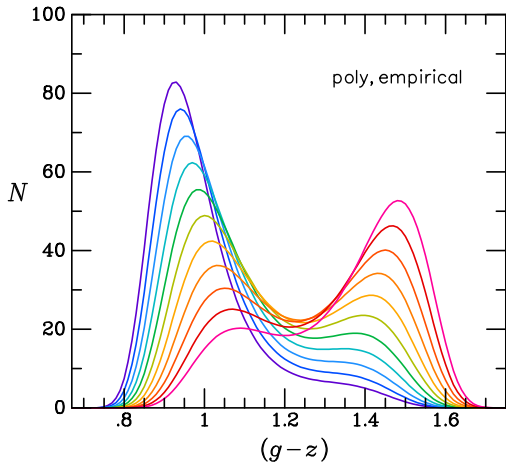


FIG. 2.— Calculated $(g-z)$ color distributions based on the empirical polynomial fit in Fig. 1 for a series of unimodal Gaussian $[\text{Fe}/\text{H}]$ distributions having a common dispersion of 0.5 dex and means ranging from -1.2 to -0.2 dex in steps of 0.1 dex. The normalization of the curves is arbitrary; the color ranges from violet/blue at low metallicity to red/magenta at high metallicity. Although the mean color increases with metallicity and the peaks shift redward, the position of the trough remains fairly constant near the point where the derivative of the metallicity with respect to color has a minimum.

tributions and MMRs include $(B-I)$ (e.g., Harris et al. 2006; Harris 2009), $(V-I)$ (Peng et al. 2009), $(B-R)$ (Spitler et al. 2006; Cantiello et al. 2007), $(g-i)$ (Wehner et al. 2008), and $(C-T_1)$ (Forte et al. 2007; Lee et al. 2008). The empirical metallicity dependencies of these indices have not been characterized in the same detail as $(g-z)$; usually the conversions to metallicity are based on simple linear approximations. However, CB07 present color-metallicity predictions in the $UBVRIZJK$ bandpasses from the Teramo “SPoT” models⁵ (Raimondo et al. 2005) and make comparisons to other SSP models in the context of color-metallicity relations. Figure 1 also shows the color-metallicity predictions from the 13 Gyr SPoT models for $(B-I)$, the color index which first revealed the presence of the MMR in the GCs of giant ellipticals (Harris et al. 2006), along with simple polynomial and cubic spline fits to the models. (The age of 13 Gyr is the same as for the models used by Yoon et al. [2006] and CB07.) The plotted $(g-z)$ and $(B-I)$ relations provide empirical and theoretical examples of nonlinear color-metallicity relations for use in this study. See Yoon et al. (2006) for a theoretical $(g-z)$ -metallicity relation and CB07 for predicted relations in other bandpasses.

2.2. Mass–Metallicity Scaling

There is evidence that the MMR is already present near the peak of the GC luminosity function (GCLF), although it is more prominent a couple magnitudes brighter than this (e.g., Harris et al. 2006; Mieske et al. 2006; Peng et al. 2009). Using linear color-metallicity relations for blue GCs, these studies derive scaling relations between GC luminosity L and metallicity Z consistent with $Z \sim L^{0.5}$ for massive elliptical galaxies (e.g., Cockcroft et al. 2009; Strader & Smith 2008), or a slope of -0.2 dex mag^{-1} for $[\text{Fe}/\text{H}]$ (we confine the discussion here to solar-scaled models). This coefficient is not observationally well constrained, as the galaxy-to-galaxy scatter is large and the applied color-metallicity conversions are approximate.

We implement this MMR scaling by assuming that the Z distribution function (ZDF) is a Gaussian in the logarithm

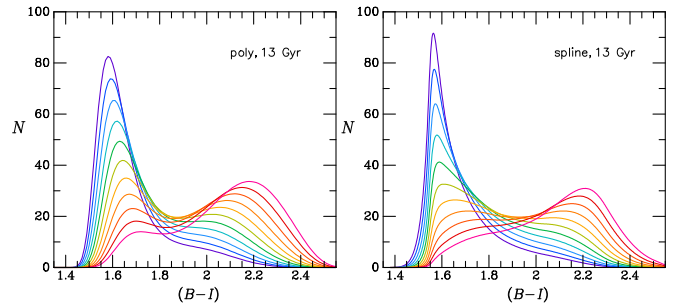


FIG. 3.— $(B-I)$ color distributions given by the polynomial (left) and spline (right) fits to the model points in Fig. 1 for a series of unimodal Gaussian $[\text{Fe}/\text{H}]$ distributions having a common dispersion of 0.5 dex and means ranging from -1.2 to -0.2 dex in steps of 0.1 dex. The normalization of the curves is arbitrary; the color ranges from violet/blue at low metallicity to red/magenta at high metallicity. Although the polynomial and spline fits to the model points in Fig. 1 are very similar, the derived color distributions depend on their derivatives and thus show marked differences. For real populations, observational errors would largely obscure such differences.

with $\sigma_{[\text{Fe}/\text{H}]} = 0.5$ dex (e.g., Yoon et al. 2006; CB07) at each magnitude, but with the mean $[\text{Fe}/\text{H}]$ increasing by 0.2 dex per magnitude brighter than the GCLF peak, up to some limit (see Sec. 2.3). Figure 2 shows the predicted $(g-z)$ color distributions for Gaussian ZDFs with $\sigma_{[\text{Fe}/\text{H}]} = 0.5$ dex and means varying from -1.2 to -0.2 dex. Consistent with the observations (e.g., P06), even at low mean metallicities there is a substantial “red tail” to the color distribution; moreover, the distribution always appears distinctly bimodal at the highest metallicities appropriate to GC systems, i.e., the blue peak is always present.

Figure 3 presents the corresponding plots for $(B-I)$ based on the polynomial and spline fits to the SPoT model predictions. We show both sets of curves to illustrate the fact that since the color distributions depend on the derivative of the nonlinear relation between metallicity and color, the interpolation method can affect the details of the derived distributions. In practice, observational errors would obscure most of these details. For the analysis below, we concentrate on the results derived using the polynomial interpolation to be more consistent with the approach used for the empirical $(g-z)$ relation (for which spline interpolation is not a reasonable option). However, we have carried out the analysis using both methods, and the results are qualitatively the same. In this case, the uncertainties and limitations of the model predictions are greater than the differences due to the interpolation scheme.

The GCs in the simulations follow a standard Gaussian GCLF at any given metallicity. Since the MMR is most prominent in giant ellipticals, we use a GCLF width $\sigma_{\text{LF}} = 1.4$ mag, characteristic of the most luminous galaxies (e.g., Harris 1991; Blakeslee et al. 1997; Harris et al. 2009), except in the discussion of the MMR for dwarf ellipticals in Sec. 3.2 below. We apply the model mass-to-light values to obtain the correct relative luminosities at different metallicities, so that the overall population follows a single Gaussian distribution in mass (e.g., Ashman et al. 1995).

2.3. Monte Carlo Simulations

The main adjustable parameters in this analysis are the mean $[\text{Fe}/\text{H}]$ at the peak of the GCLF, which we label $\langle[\text{Fe}/\text{H}]\rangle_0$, and the maximum mean metallicity that we allow for the brightest GCs, which we label $\langle[\text{Fe}/\text{H}]\rangle_{\text{max}}$. In other words, we impose a fixed mean of $\langle[\text{Fe}/\text{H}]\rangle_{\text{max}}$ for the ZDF of the GCs above some luminosity limit, rather than continuing the scaling relation indeterminately. The mean $[\text{Fe}/\text{H}]$ of the

⁵ <http://www.oao-teramo.inaf.it/SPoT>

GC system could be derived from $\langle[\text{Fe}/\text{H}]\rangle_0$, $\langle[\text{Fe}/\text{H}]\rangle_{\text{max}}$, and the GCLF. Empirically, the mean GC metallicity increases with galaxy luminosity (Côté et al. 1998; P06). We do not explicitly include galaxy properties in these simulations, but we consider a large enough range in $\langle[\text{Fe}/\text{H}]\rangle_0$ and $\langle[\text{Fe}/\text{H}]\rangle_{\text{max}}$ to make useful comparisons to galaxies with a range of luminosities.

Given the above set of assumptions, we generate random realizations of GC systems and examine their color distributions and color-magnitude relations. We simulate realistic observational scatter by adding random magnitude errors that scale exponentially as $\sigma_m \sim 10^{-0.4m}$, and we set the normalization such that the color error at the GCLF peak is 0.1 mag. We also include an additional 0.01 mag scatter at all magnitudes, which could represent errors in aperture corrections or intrinsic scatter in the GC colors at fixed metallicity. We experimented with larger values of these errors, but we note that the blue tilt is only detectable with the best available photometric data and analyses, and we do not wish to obscure the effect we are trying to characterize.

2.4. Color-Magnitude Fitting Procedure

To characterize the blue (and red) tilts in our simulated samples, we basically follow the procedure described in Mieske et al. (2006), which is similar to that used in other studies (e.g., Peng et al. 2009). Specifically, we bin the GCs by magnitude, using a minimum bin size of 0.2 mag but allowing the size in magnitudes to increase in order to contain at least 200 GCs per bin. We then use the heteroscedastic mode of the KMM mixture modeling algorithm (Ashman et al. 1994) to determine the peaks of the color distributions for the different bins. We perform linear fits to determine how the peak positions vary as a function of magnitude. The fits are done using all bins that are more than $1\sigma_{\text{LF}}$ brighter than GCLF turnover magnitude; for giant ellipticals this is close to the “million solar mass” threshold (Harris 2009) where the tilt becomes noticeable in observational data. The following section presents the results for the color-magnitude slopes for the blue and red peaks in these simulations.

3. RESULTS

3.1. Blue vs Red Tilts for Baseline Models

Figure 4 plots the slope of the blue peak in the $(g-z)$ color distribution determined by KMM as a function of magnitude versus the corresponding slope for the red peak. Each panel shows results for 101 random realizations of a GC population with 10,000 members brighter than the GCLF peak. The twelve different panels are for different combinations of $\langle[\text{Fe}/\text{H}]\rangle_0$ and $\langle[\text{Fe}/\text{H}]\rangle_{\text{max}}$, defined in Sec. 2.3; their values are shown in each panel. In particular, the mean metallicity at the GCLF peak $\langle[\text{Fe}/\text{H}]\rangle_0$ is varied from -1.0 dex (one-tenth solar) to -0.5 dex (one-third solar), but only two values, -0.3 (half solar) and 0.0 (solar), are shown for the maximum mean metallicity parameter $\langle[\text{Fe}/\text{H}]\rangle_{\text{max}}$. Lower values of $\langle[\text{Fe}/\text{H}]\rangle_{\text{max}}$ decrease the mean metallicity range of the MMR to factors of only ~ 2 and/or restrict the simulated populations to lower mean metallicities and bluer mean colors than those found in the giant ellipticals where the “blue tilt” is commonly observed. Setting $\langle[\text{Fe}/\text{H}]\rangle_{\text{max}}$ to values above solar metallicity (or removing it altogether) gives results similar to the case with $\langle[\text{Fe}/\text{H}]\rangle_{\text{max}} = 0.0$ dex, already a high metallicity for GCs. Thus these two values of $\langle[\text{Fe}/\text{H}]\rangle_{\text{max}}$ prove adequate for our purposes.

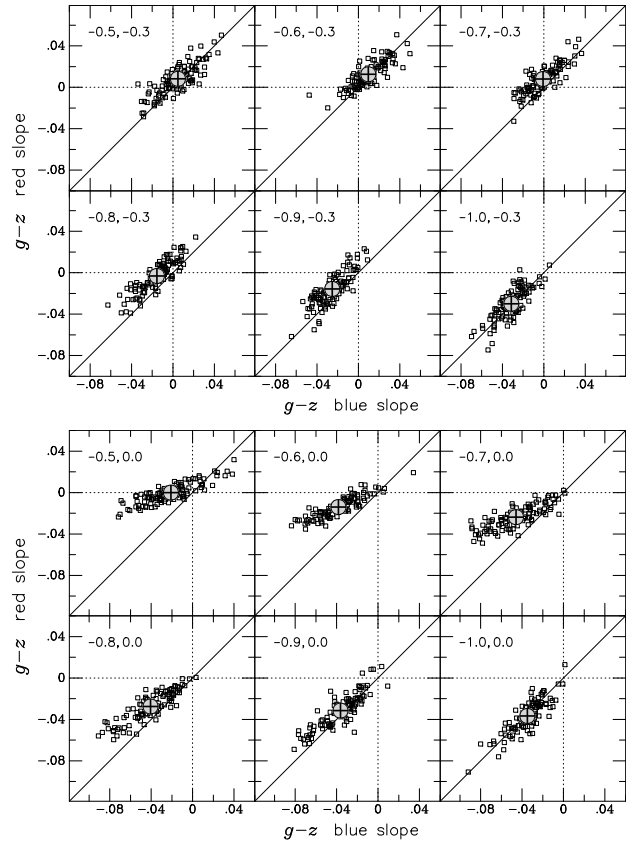


FIG. 4.— Blue versus red tilts in simulated GC $(g-z)$ color distributions. Each point represents the slopes of the blue and red peak colors determined by KMM fits as a function of magnitude within a single realization of a population of 10,000 GCs. See text for details on KMM fitting. Each panel shows the slopes for 101 different realizations (squares), all with the same model parameters. The large encircled crosses mark the average values. From panel to panel, we vary two parameters: $\langle[\text{Fe}/\text{H}]\rangle_0$, which is the mean metallicity for GCs at the mean luminosity of the GCLF, and $\langle[\text{Fe}/\text{H}]\rangle_{\text{max}}$, which is mean metallicity of the most luminous GCs in the population. The values of these parameters in dex are displayed in the upper left of each panel; for reasons given in the text, we show results for only two values of $\langle[\text{Fe}/\text{H}]\rangle_{\text{max}}$. At any given luminosity, the GCs follow a unimodal metallicity distribution of width $\sigma_{[\text{Fe}/\text{H}]} = 0.5$ dex. Here we use $\sigma_{\text{LF}} = 1.4$ mag for the GCLF width, appropriate for massive early-type galaxies. We note that several of these panels show a strong preference for “blue tilts,” i.e., negative blue-peak slopes that are significantly larger in absolute value than the red-peak slopes.

The points in Figure 4 with negative slope values are the ones that show a reddening of the peak colors with increasing luminosity; thus, these are the populations that would empirically be described as having a positive MMR. The third row of panels in Figure 4 is particularly interesting, as the blue-peak slopes are generally larger in absolute value than the red-peak slopes. For example, in the three panels of Figure 4 with $\langle[\text{Fe}/\text{H}]\rangle_{\text{max}} = 0.0$ and $\langle[\text{Fe}/\text{H}]\rangle_0 = -0.5, -0.6, -0.7$ dex, the mean $(g-z)$ blue-peak slopes are $\langle d(g-z)/dz \rangle_B = -0.023, -0.039, -0.046$, respectively, and the red-peak slopes are $\langle d(g-z)/dz \rangle_R = -0.001, -0.014, -0.024$. The scatter in these slope values is typically ~ 0.02 , so the uncertainties on the mean slopes are about ± 0.002 . If a linear transformation were used to convert the slopes from color to metallicity, the conclusion would be that the blue GCs have a stronger MMR, but this is not the case here, where there is a single MMR and no bimodality in metallicity. For comparison, analysis of a combination ACS Virgo and Fornax Cluster Survey (Côté et al. 2004; Jordán et al. 2007a) galaxies gives

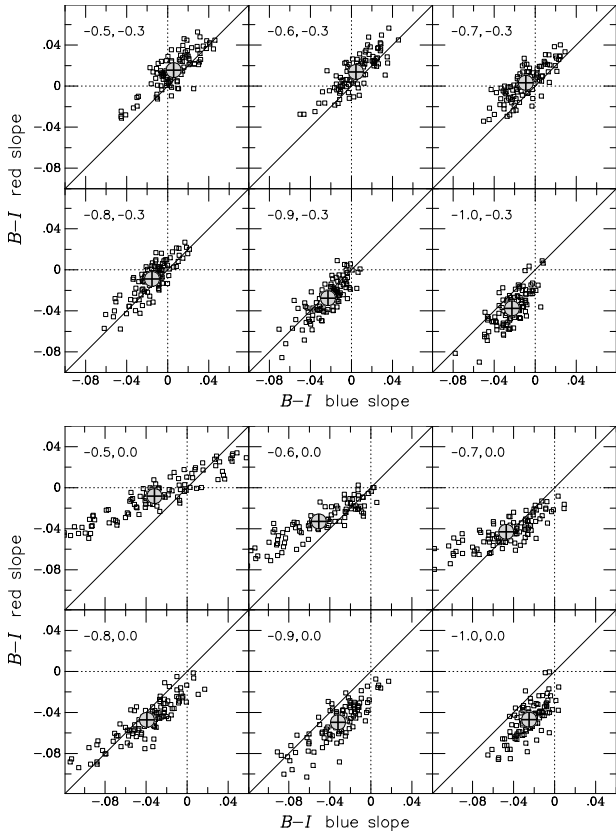


FIG. 5.— Same as Fig. 4, but here shown for the slopes with mag of the fitted KMM blue and red peaks in the simulated GC $(B-I)$ color distributions.

mean $(g-z)$ blue and red peak slopes of -0.035 ± 0.008 and -0.016 ± 0.010 , respectively, with substantial scatter among different subsamples (Mieske et al. 2010). Thus, the simulation with $\langle[\text{Fe}/\text{H}]_0\rangle, \langle[\text{Fe}/\text{H}]_{\text{max}}\rangle = -0.6, 0.0$ dex provides a very good match to the observed $(g-z)$ blue and red tilts.

Even for the top two rows of panels in Figure 4, there is a general preference for blue tilts over red ones. More specifically, where both blue and red slopes are negative, there is a tendency for the blue slope to be more negative, that is, to have a more pronounced color-magnitude relation. For example, the simulation with $\langle[\text{Fe}/\text{H}]_0\rangle, \langle[\text{Fe}/\text{H}]_{\text{max}}\rangle = -0.9, -0.3$ (second row, middle panel) has mean $(g-z)$ blue and red slopes of -0.025 ± 0.002 and -0.016 ± 0.002 , respectively. We choose this as a lower metallicity comparison because it has the same factor-of-four range in the MMR limits and also favors the blue tilt, though to a lesser degree.

Figure 5 presents analogous results from the same set of simulations but for the slopes of the blue and red peaks of the $(B-I)$ color distributions with magnitude. As described above, the transformation from metallicity to $(B-I)$ colors is based on the 13 Gyr Teramo SPoT models, whereas the $(g-z)$ colors are from the P06 empirical transformation. Overall, the results are fairly similar, but the tendency to favor blue tilts is somewhat weaker among these simulations using the model-based transformations. In this case, the model with $\langle[\text{Fe}/\text{H}]_0\rangle, \langle[\text{Fe}/\text{H}]_{\text{max}}\rangle = -0.6, 0.0$ (second row, middle panel) has mean blue and red slopes $\langle d(B-I)/dI \rangle_B = -0.049 \pm 0.003$ and $\langle d(B-I)/dI \rangle_R = -0.032 \pm 0.002$. The blue slope is very similar to the value of -0.05 found by Harris (2009), but that study found no significant red slope, although Bailin & Harris (2009) state that it should present at some level. For the

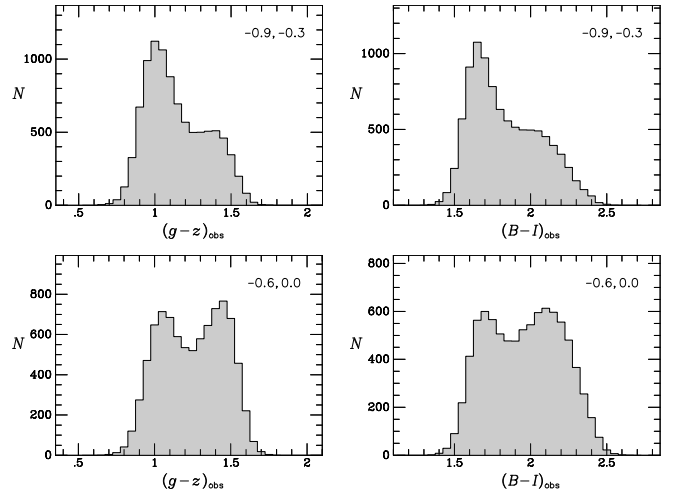


FIG. 6.— Example histograms of $(g-z)$ and $(B-I)$ colors for GCs in two simulated populations with values of $\langle[\text{Fe}/\text{H}]_0\rangle$ and $\langle[\text{Fe}/\text{H}]_{\text{max}}\rangle$ given in the upper right of each panel. The top panels are typical of the GC color distributions for intermediate luminosity galaxies, while the lower panels resemble the distributions for the most massive early-type galaxies (e.g., Peng et al. 2006). Both of these simulations show a tendency towards blue tilts for the $(g-z)$ colors; only the higher metallicity model tends towards blue tilts for the $(B-I)$ colors, which are derived from a model, rather than empirical, color-metallicity relation.

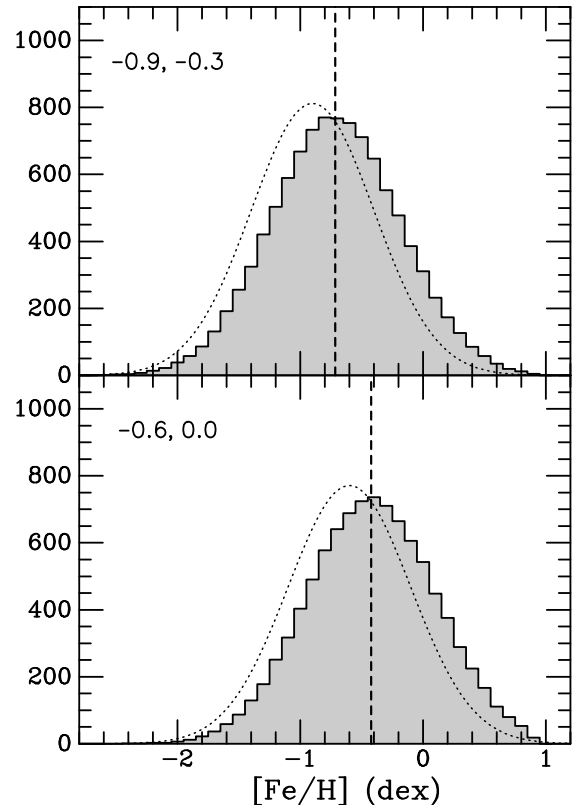


FIG. 7.— Metallicity distributions (grey histograms) for the simulations whose color histograms are displayed in Figure 6. We plot metallicities only for model GCs brighter than the GCLF peak, since there is no mass-metallicity scaling at fainter luminosities. Including the fainter half of the GCLF would shift the peak value lower by ~ 0.08 dex. For comparison, the dotted curves show Gaussian metallicity distributions with mean = $\langle[\text{Fe}/\text{H}]_0\rangle$, $\sigma_{[\text{Fe}/\text{H}]} = 0.5$, and normalized to have the same total areas as the histograms. The dashed lines mark the mean metallicities of the plotted histograms.

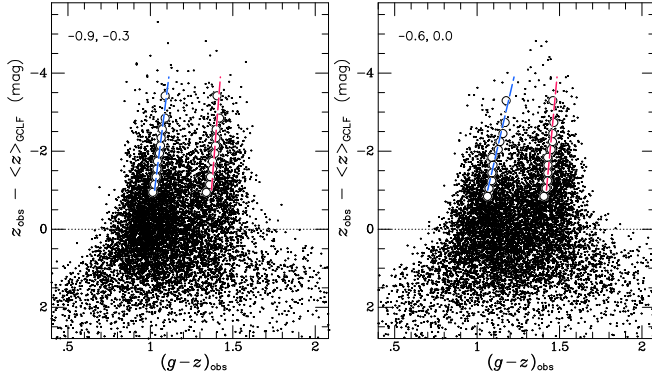


FIG. 8.— Color-magnitude diagrams for two simulations discussed in the text. The values of $\langle [Fe/H] \rangle_0$ and $\langle [Fe/H] \rangle_{\max}$ are shown, and the magnitudes are given with respect to the GCLF mean. We plot points for 10,000 GCs in each simulation. The large circles show the results from the KMM fits, which are based on 20 times the number of GCs as are plotted in these panels. The dashed blue and red lines are linear fits to the KMM peak results. These diagrams are illustrative, but in real populations there may be unmodeled correlations of mean GC metallicity and color with galaxy luminosity, GCLF width, or other parameters.

model with $\langle [Fe/H] \rangle_0, \langle [Fe/H] \rangle_{\max} = -0.9, -0.3$, the blue and red slopes are -0.021 and -0.026 , respectively, so the red tilt is greater in this case, although neither is very large. Despite this, we consider it an interesting lower-metallicity comparison model on account of the empirically-based $(g-z)$ slopes discussed above.

Figure 6 presents example $(g-z)$ and $(B-I)$ histograms for the two models we have been discussing. These histograms exemplify the range of color distributions typically found in intermediate- to high-luminosity elliptical galaxies. The distributions are clearly bimodal in all the panels of this figure. In the top panels the blue peak dominates, giving an appearance very similar to the GC color distributions found by P06 for Virgo galaxies with $M_B \approx -19$ mag. On the other hand, the roughly equal peaks in the histograms of the lower panels of Figure 6 are quite similar to those found for the most massive early-type galaxies (e.g., P06; Harris et al. 2006). These are the galaxies that also show the blue tilt most strongly. It is interesting that galaxies with relatively more dominant blue peaks would have weaker blue tilts; this would be puzzling for a trivial linear conversion between color and metallicity. However, as shown by the slope-slope comparisons in Figures 4 and 5, the more realistic color-metallicity conversions used here reproduce this observational finding.

In comparison to the color histograms, Figure 7 shows that despite the MMR built into the models, the underlying metallicity distributions still appear unimodal. Thus, the bifurcation in color results purely from the nonlinearity of the color-metallicity conversion, not the varying of GC mean metallicity with luminosity. Figure 8 illustrates the z versus $(g-z)$ color-magnitude diagrams for these baseline models. For clarity, the plotted simulations contain 10,000 GCs each. The larger circles show results from KMM fits as described in Sec. 2.4. In order to delineate the trends more clearly, the KMM fits in Figure 8 are based on 20 times the number of GCs as are plotted in the panels. As with the color histograms, these color-magnitude diagrams bear a good resemblance to those found observationally (e.g., P06, Mieske et al. 2006).

3.2. Dwarf Galaxies: the Effect of the GCLF

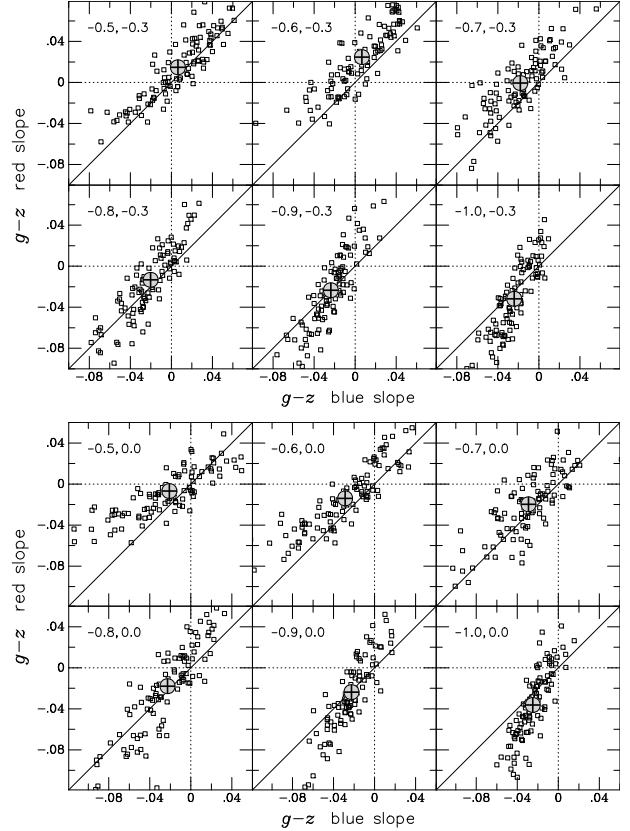


FIG. 9.— Same as Fig. 4, but here shown for sets of simulations using $\sigma_{\text{LF}} = 0.9$ mag, typical of the GCLF widths of dwarf galaxies. Although some individual realizations may have large “tilts” (slopes), the scatter is large and encompasses $(0, 0)$ at the $\lesssim 1\sigma$ level. Thus, there is no significant tendency for either red or blue tilts.

Observationally, the color-magnitude relation of blue-peak GCs is mainly a property of giant ellipticals, and the trend is weak or absent in lower luminosity galaxies (e.g. DeGraaff et al. 2007; Cantiello et al. 2007). However, Mieske et al. (2006, 2010) have detected it in pooled samples of GCs from faint early-type galaxies. As we have shown, the simulations with lower metallicity, which are more appropriate to low luminosity ellipticals, have less of a tendency to favor the blue tilt than do the higher metallicity simulations. However, the likely more important reason for the lack of strong blue tilts in dwarf galaxies has to do with their GCLFs. Not only do they have many fewer GCs, but their luminosity functions are narrower. If the GCLF is too narrow, the GCs will not reach high enough luminosities to evince a significant MMR.

Jordán et al. (2006) found that the width of the GCLF decreases linearly with magnitude. For early-type galaxies with $M_B \gtrsim -18$, the width $\sigma_{\text{LF}} \lesssim 0.9$ mag; this includes the majority of the ACS Virgo and Fornax Survey galaxies, which are actually dominated by dwarf ellipticals. Figure 9 shows results for the slopes with magnitude of the peaks in the $(g-z)$ color distributions analogous to Figure 4, but for populations with a narrower GCLF $\sigma_{\text{LF}} = 0.9$ mag, appropriate to dwarf ellipticals. The scatter in the slope values is roughly a factor of two larger for the case with $\sigma_{\text{LF}} = 0.9$ as compared to $\sigma_{\text{LF}} = 1.4$, and encompasses $(0, 0)$ at the $\lesssim 1\sigma$ level in all cases. Measurements of the slopes in individual realizations are generally not significant at more than the 1σ level. Thus, the lower metallicities and narrower GCLF can explain why

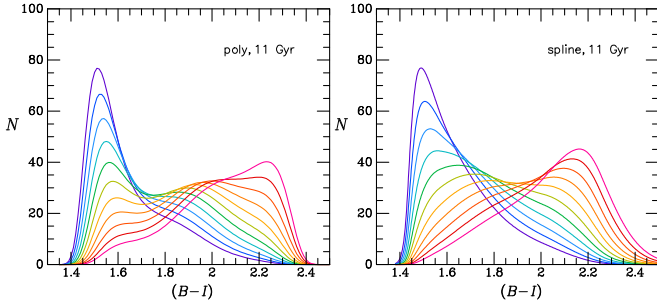


FIG. 10.— Similar to Fig. 3, but here based on the color–metallicity predictions from the 11 Gyr SPoT models. Compared to the 13 Gyr models, there are more significant differences in the color distributions derived here from the polynomial and spline fits. A more complete set of model metallicities would help alleviate this interpolation uncertainty.

the observed GC color–magnitude trends are very weak in low luminosity galaxies.

3.3. Age Issues

So far the discussion has centered on GC color distributions from simulations using the empirical ($g-z$)–metallicity relation and a theoretical ($B-I$)–metallicity relation from the 13 Gyr SPoT models. As shown previously in Figures 2 and 3, both of these produce clearly bimodal color distributions from single Gaussians in metallicity. As another example, Figure 10 shows predicted ($B-I$) distributions similar to those in Figure 3 but now based on the 11 Gyr SPoT models. The agreement between the distributions derived with the polynomial and spline interpolations is worse here than for the 13 Gyr models, mainly because the polynomial fit is poorer. At the highest metallicities, the polynomial-derived curves in Figure 10 appear almost trimodal, whereas the spline-derived curves appear fairly similar to those in Figure 3, except that the blue peak is a bit broader.

To examine the effects of these more irregular color distributions, Figure 11 shows results for the slopes of the peaks in the ($B-I$) color distributions analogous to Figure 5, but based on the polynomial fits to the color–metallicity relations from the 11 Gyr SPoT models. The scatter is higher by at least $\sim 50\%$, and in some cases several times larger, because the distributions are less clearly bimodal, making the KMM fits much less robust. As in the case for the 13 Gyr models, there is no clear preference for blue tilts in the two rows of panels in Figure 11 with $\langle[\text{Fe}/\text{H}]\rangle_{\text{max}} = -0.3$ dex. However, there is a tendency towards blue tilts in the third row of panels, in the sense that the slopes are negative and the blue slopes tend to be greater in absolute value than the red slopes. In particular, for our fiducial “giant galaxy” model with $\langle[\text{Fe}/\text{H}]\rangle_0, \langle[\text{Fe}/\text{H}]\rangle_{\text{max}} = -0.6, 0.0$ dex, the mean blue and red slopes are $\langle d(B-I)/dI \rangle_B = -0.059 \pm 0.005$ and $\langle d(B-I)/dI \rangle_R = -0.022 \pm 0.003$. This indicates an even stronger blue tilt than for the 13 Gyr models, though again with much larger scatter. Unfortunately, the behavior of the color–metallicity relation as a function of age is not well calibrated, and as we have seen, the results in this case depend on the interpolation method. Of course, the ($g-z$) results based on the empirical color–metallicity transformation do not explicitly assume any age for the GCs, and the simulated ($g-z$) distributions are strongly bimodal with a clear tendency for the blue tilt.

We further note that since the point of inflection of the nonlinear color–metallicity relation shifts with age, it is also possible to introduce a blue tilt by making the brightest GCs

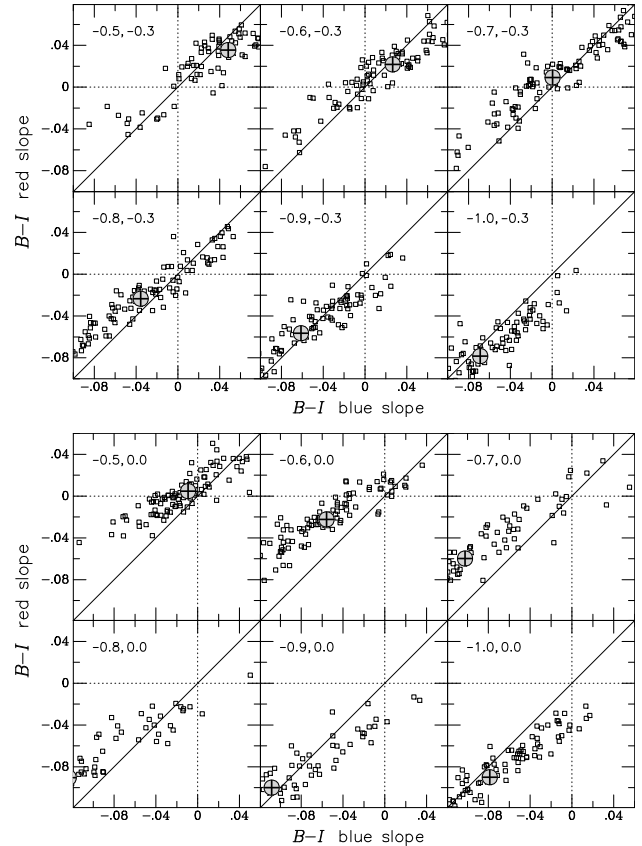


FIG. 11.— Same as Fig. 5, but here based on color–metallicity relations from the 11 Gyr models (using the polynomial fits to the color–metallicity relation, as in Fig. 5).

have systematically older ages (S.-J. Yoon, private communication). However, there is no a priori reason to assume a gradient in age with luminosity, whereas the MMR that we have used in our simulations is reasonable based on GC self-enrichment. Related to this, it would be very useful to have observations of GC color distributions at various lookback times to see how the color bimodality changes with time. If there is underlying bimodality in metallicity, it should change very little. On the other hand, if it is due to the inflection in the color–metallicity relation, then the bimodality should decrease even at modest lookback times of a few Gyr (e.g., compare Figures 3 and 10). In practice, the observational requirements are forbidding, since it involves measuring precise GC color distributions at $z \gtrsim 0.2$.

Kalirai et al. (2008) attempted to measure evolution in the GC colors of a $z=0.089$ elliptical galaxy serendipitously observed in extremely deep *HST* imaging of a foreground Galactic globular cluster. These authors detected two peaks in the color distribution and interpreted them as the usual local peaks, but shifted substantially *redder* at $z=0.089$ (even after extinction and k corrections). Large *anti*-evolution in color at a lookback time of just over 1 Gyr would not be easy to understand in the context of either explanation for color bimodality. However, from Fig. 2 of Kalirai et al., it appears that the true blue and red peaks are probably where they should be, but they are unresolved because of observational error at these faint magnitudes. The apparent red peak in the color distribution is likely contamination from the coolest members of the white dwarf sequence in the foreground cluster. Thus, this

study illustrates the difficulty of such observations. However, it would be worth trying this experiment with the next generation of astronomical observatories, such as the *James Webb Space Telescope (JWST)* and ground-based extremely large telescopes (ELTs). In the meantime, further refinements in the model color-metallicity predictions for different ages and elemental abundance ratios are greatly needed.

4. DISCUSSION: BIMODALITY OR NONLINEARITY?

The nonlinear dependence of GC optical colors on metallicity is found both empirically and from detailed SSP modeling. Because the observed and predicted relations naturally produce bimodal color distributions, this nonlinearity is the simplest explanation for the observed universality of bimodal color distributions. The simplicity of this explanation is the strongest argument in its favor. In contrast, *universal* bimodality in the underlying GC metallicity distributions would be difficult to understand in the context of hierarchical formation models. However, this argument is purely a theoretical bias, and it is important to critically examine the available data. Of course, even if the nonlinearity is the principal cause of the characteristic double-peaked GC color histograms, this would not preclude a predominance of two distinct metallicity components in *some* galaxies.

For the models explored in the present work, there is no bimodality in metallicity, just a subtle increase in the mean GC metallicity with mass, as may be expected from self-enrichment models. We have done this precisely to test whether or not the ‘blue tilt’ can occur within unimodal metallicity distributions. As we have shown, the resulting color distributions and color-magnitude relations are similar to those found in real galaxies. The correlation between luminosities and metallicities in these models is dominated by scatter, as shown in Figure 12, which plots the z -band magnitude-metallicity relation that would be observed for our favored giant elliptical model. The plotted ‘observed metallicities’ in the right panel of Figure 12 are found by using the colors that include simulated observational error and then inverting the color-metallicity relation. The resemblance of this figure to the corresponding one observed by Mieske et al. (2006, see their Fig. 12) is striking.

Very little is actually known about the detailed metallicity distributions of GCs in giant ellipticals. In support of their hypothesis, Yoon et al. (2006) showed that the histogram of M_{gb} values for 150 GCs in M87 from Cohen et al. (1998) is reasonably consistent with a Gaussian metallicity distribution and the conversions predicted by their SSP models; however, this represents only 1% of the GCs and may not be representative of the full population. In contrast, Strader et al. (2007) found that metallicities derived from the Lick index measurements for 47 GCs in M49 (Cohen et al. 2003) do appear bimodal, in the sense that a double Gaussian provided a significantly better fit to their derived metallicities than a single Gaussian. A skewed distribution, such as found for halo stars in other galaxies (e.g., Harris & Harris 2002; Harris et al. 2007) and derived by Yoon et al. (2010) from multi-band optical photometry of extragalactic GC systems, would also favor two-Gaussian models, even if the enrichment process was continuous. Perhaps more importantly, this 47-object spectroscopic sample represents only $\sim 0.6\%$ of M49’s total population. It may be that such a small sample of bright

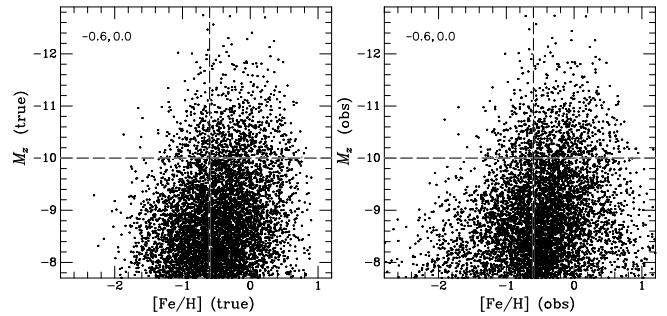


FIG. 12.— Magnitude-metallicity relation for a simulated population of 10,000 GCs with metallicity range parameters $(\langle[Fe/H]\rangle_0, \langle[Fe/H]\rangle_{\max}) = (-0.6, 0.0)$ and $\sigma_{LF} = 1.4$ mag, our fiducial ‘giant galaxy’ model. *Left*: true z -band magnitudes and metallicities for GCs in the simulation. *Right*: model ‘observed’ magnitudes and the metallicities inferred from the $(g-z)$ colors, including simulated observational error. Consistent with empirical studies, there is no well-defined trend of the observed magnitude with metallicity in the overall population; the right panel can be compared to Fig. 12 of Mieske et al. (2006), to which it bears a strong resemblance. The dashed fiducial lines are the same as those in Mieske et al.: the horizontal line marks the approximate magnitude where the ‘tilt’ becomes more pronounced, and the vertical line approximates the mean metallicity of the GCs fainter than this.

GCs observed in two spectroscopic masks in two regions of M49 shows metallicity bimodality, but that the full population would have a more continuous distribution from the blending of numerous substructures and metallicity components as expected from hierarchical accretion. We note that the metallicities as published by Cohen et al. for the same sample of GCs do not strongly favor bimodality (KMM p -value = 0.10), even though they come from the same data and correlate well with those of Strader et al. (2007). This is because subtle changes in a few metallicities can have large effects on the interpretation when the sample size is small. In another study, Puzia et al. (2005) presented spectroscopic metallicities, ages, and $[\alpha/Fe]$ ratios for 71 GCs in seven early-type galaxies, finding evidence for trends of decreasing GC age and $[\alpha/Fe]$ with increasing metallicity. The metallicity histogram for this sample appeared unimodal, but with broad tails (see Fig. 7 of Puzia et al. 2005). In short, published spectroscopic data sets are inadequate for detailed constraints on the GC metallicity distributions in the general population of early-type galaxies.

The prospects for obtaining large samples are of course more favorable with multi-band imaging, and the combination of high-quality near-IR and optical photometry can provide useful constraints on metallicity (see CB07). For instance, by combining optical and IRAC 3.6 μm -band photometry for 146 GCs in the peculiar, post-merger elliptical NGC 5128 (Cen A), Spitler et al. (2008) found evidence for bimodality in metallicity. A similar data set for 75 GCs in the Sombrero galaxy was inadequate to draw any conclusions in this regard. Several other important, ground-breaking studies of the optical-IR colors of GCs in giant ellipticals have been carried out (e.g., Kissler-Patig et al. 2002; Puzia et al. 2002; Hempel et al. 2007). The color distributions generally appear broad, often with non-Gaussian tails, but the samples are still relatively small and do not show the same obvious bimodality as found in the large samples of purely optical GC colors. A claimed exception to this was based on matched WFPC2 I and NICMOS H photometry of a pruned subsample of 80 GCs in M87 (Kundu & Zepf 2007). The positions and photometry for these objects were never published, but the histogram showed a gap at intermediate color. However, the red ‘peak’ comprised an excess of only 4 GCs with respect to this gap, and a double Gaussian was preferred over a single

Gaussian at only the $2.4\text{-}\sigma$ level. Most importantly, the whole sample constituted only 0.5% of the full population of M87 GCs. Representative samples of optical-IR GC colors in a statistical number of elliptical galaxies are needed for general constraints on their metallicity distributions. In addition, the establishment of empirical conversions from these colors to metallicity, and detailed comparison to model predictions as a function of age, will be essential. Several groups are actively working on this topic, so the data required for these efforts should be available in the near future.

5. CONCLUSIONS

The combination of a realistic, nonlinear color-metallicity dependence with a simple mass-metallicity scaling relation motivated by self-enrichment considerations can produce GC populations with bimodal color distributions *and* an apparent color-magnitude relation (“blue tilt”) for the GCs within the blue peak of the color distribution. The underlying metallicity distributions are unimodal. For certain metallicity ranges, the color-magnitude relation for GCs within the red peak is weak or absent, consistent with observations for most giant elliptical galaxies. The models which reproduce these features have nearly equal red and blue peaks, again consistent with the data for giant ellipticals. As noted by Yoon et al. (2006), this equality occurs because the inflection point in the color-magnitude relation is approximately equal to the peak metallicity of the GC system. It is when the peak metallicity begins to move through the inflection point that the “blue tilt” becomes most pronounced. As a result, the significance of the tilt tends to increase in higher metallicity populations with redder mean colors; thus, it would be greater in more massive galaxies and at smaller galactocentric radii, both of which are found observationally (Mieske et al. 2006, 2010).

At the low-metallicity extreme of our simulations, there is actually a preference for red tilts over blue ones because the peak of the metallicity distribution is well below the inflection point of the color-metallicity relation. But in practice, the galaxies that would harbor such metal-poor systems would have low luminosities, few GCs, and far too few red GCs to show a significant tilt. The narrower GCLFs typical of low-luminosity galaxies also greatly reduce the significance of any color-magnitude trends in our simulations because of the reduced range in GC luminosity. Further, because we have assumed a single mass-metallicity relation for all GCs, this scenario implies that the redder, more metal-rich GC systems of giant galaxies will have a higher mean mass than those of dwarf ellipticals, again consistent with observations (Jordán et al. 2007b).

A few giant galaxies with weak or absent blue tilts such as M49 (Mieske et al. 2006; Strader et al. 2006; but see also Lee et al. 2008) can be understood as simply being consistent with stochastic variations among different model realizations. This is because the actual underlying metallicity distribution is broad. If the colors linearly reflected metallicity, so that the blue peak of the GC color distribution truly represented a distinct subpopulation “squeezed” into a narrow metallicity margin that tightly became more metal-rich with luminosity, then stochastic variations in such a homogeneous population would be small. Thus, a large galaxy without a blue tilt would be truly anomalous. However, even in our favored high-metallicity model that accurately reproduces the observed mean ($g-z$) blue and red tilts, at least 15% of the simulations lack significant color-magnitude slopes in the blue peak. Thus, it is not surprising to find a galaxy like

M49, and this scenario predicts that others will be found once large samples of giant ellipticals with similarly well-measured color-magnitude diagrams are available.

Further observations are needed to test this scenario more quantitatively. In particular, we still do not know in detail the underlying form of the metallicity distributions of GCs in giant ellipticals, and we have assumed Gaussians only for the sake of simplicity, whereas the true distributions may be skewed in a manner similar to that of old halo stars (Yoon et al. 2010). Accurate characterization of these distributions will require still larger spectroscopic samples and improved models for converting measured indices to actual metallicities. As we have noted, large samples of optical-IR colors in multiple elliptical galaxies, and empirical conversions from these colors to metallicity, are also needed. The required data should be available soon from ongoing observational efforts.

We have found that the precise shapes of GC color distributions can depend on the fine details of the color-metallicity conversion. In addition to more extensive data samples, improving the accuracy of photometrically estimated GC metallicities will require a broader and more densely calculated set of models, all with better calibrations against resolved stellar populations. The variation of alpha-element enhancement as a function of metallicity needs to be calibrated and taken into account for accurate data-model comparisons. Further refinement in our understanding of changes in the color-metallicity relation with age, particularly with regards to the behavior of the horizontal branch, is essential. It is also important to obtain useful empirical constraints on trends in GC age with metallicity, although there will likely be large variations in any such trends due to the merging histories of individual galaxies. A still more challenging task is to measure the change in color distributions with age by obtaining high quality photometry of GC populations at significant cosmological lookback times.

Finally, we note that this investigation has explored the behavior of the blue tilt phenomenon under variations of only two parameters, here labeled $\langle[\text{Fe}/\text{H}]\rangle_0$ and $\langle[\text{Fe}/\text{H}]\rangle_{\text{max}}$. Although we consider the results presented here promising, more sophisticated models are of course desirable, especially once more precise color-metallicity transformations become available. Given the remaining uncertainties and the importance of GC metallicity distributions to understanding detailed galaxy formation histories, we hope that this will continue to be an active area of theoretical and observational research into the coming era of *JWST* and the planned ELTs.

We thank the anonymous referee for helpful comments. It is a pleasure to thank S.-J. Yoon and P. Côté for enlightening discussions. M.C. acknowledges support from ASI-INAF (program I/016/07/0), PRIN-INAF 2006 (P.I. G. Clementini), and PRIN-INAF 2008 (P.I. M. Marconi). E.W.P. gratefully acknowledges the support of the Peking University Hundred Talent Fund (985). J.P.B. thanks N.-J. Kim for providing inspiration for this work.

REFERENCES

- Ashman, K. M., Bird, C. M., & Zepf, S. E. 1994, *AJ*, 108, 2348
 Ashman, K. M., Conti, A., & Zepf, S. E. 1995, *AJ*, 110, 1164
 Ashman, K. M., & Zepf, S. E. 1992, *ApJ*, 384, 50
 Bailin, J., & Harris, W. E. 2009, *ApJ*, 695, 1082
 Beasley, M. A., Baugh, C. M., Forbes, D. A., Sharples, R. M., & Frenk, C. S. 2002, *MNRAS*, 333, 383
 Blakeslee, J. P., Tonry, J. L., & Metzger, M. R. 1997, *AJ*, 114, 482
 Blakeslee, J. P., et al. 2009, *ApJ*, 694, 556
 Brown, J. H., Burkert, A., & Truran, J. W. 1991, *ApJ*, 376, 115
 Cantiello, M., & Blakeslee, J. P. 2007, *ApJ*, 669, 982 (CB07)
 Cantiello, M., Blakeslee, J. P., & Raimondo, G. 2007, *ApJ*, 668, 209
 Cockcroft, R., Harris, W. E., Wehner, E. M. H., Whitmore, B. C., & Rothberg, B. 2009, *AJ*, 138, 758
 Cohen, J. G., Blakeslee, J. P., & Côté, P. 2003, *ApJ*, 592, 866
 Cohen, J. G., Blakeslee, J. P., & Ryzhov, A. 1998, *ApJ*, 496, 808
 Côté, P., Marzke, R. O., & West, M. J. 1998, *ApJ*, 501, 554
 Côté, P., et al. 2004, *ApJS*, 153, 223
 Côté, P., et al. 2008, *IAU Symposium*, 245, 395
 DeGraff, R. B., Blakeslee, J. P., Meurer, G. R., & Putman, M. E. 2007, *ApJ*, 671, 1624
 De Lucia, G., Springel, V., White, S. D. M., Croton, D., & Kauffmann, G. 2006, *MNRAS*, 366, 499
 Dopita, M. A., & Smith, G. H. 1986, *ApJ*, 304, 283
 Forte, J. C., Faifer, F., & Geisler, D. 2007, *MNRAS*, 382, 1947
 Gebhardt, K., & Kissler-Patig, M. 1999, *AJ*, 118, 1526
 Harris, W. E. 1991, *ARA&A*, 29, 543
 Harris, W. E. 2009, *ApJ*, 699, 254
 Harris, W. E., & Harris, G. L. H. 2002, *AJ*, 123, 3108
 Harris, W. E., Harris, G. L. H., Layden, A. C., & Stetson, P. B. 2007, *AJ*, 134, 43
 Harris, W. E., Kavelaars, J. J., Hanes, D. A., Pritchett, C. J., & Baum, W. A. 2009, *AJ*, 137, 3314
 Harris, W. E., Whitmore, B. C., Karakla, D., Okoń, W., Baum, W. A., Hanes, D. A., & Kavelaars, J. J. 2006, *ApJ*, 636, 90
 Hempel, M., Zepf, S., Kundu, A., Geisler, D., & Maccarone, T. J. 2007, *ApJ*, 661, 768
 Jefferys, W. H., Fitzpatrick, M. J., & McArthur, B. E. 1988, *Celestial Mechanics*, 41, 39
 Jordán, A., et al. 2006, *ApJ*, 651, L25
 Jordán, A., et al. 2007a, *ApJS*, 169, 213
 Jordán, A., et al. 2007b, *ApJS*, 171, 101
 Kalirai, J. S., Strader, J., Anderson, J., & Richer, H. B. 2008, *ApJ*, 682, L37
 Kissler-Patig, M., Brodie, J. P., & Minniti, D. 2002, *A&A*, 391, 441
 Kodama, T., Tanaka, I., Kajisawa, M., Kurk, J., Venemans, B., De Breuck, C., Vernet, J., & Lidman, C. 2007, *MNRAS*, 377, 1717
 Kravtsov, A. V., & Gnedin, O. Y. 2005, *ApJ*, 623, 650
 Kundu, A., & Zepf, S. E. 2007, *ApJ*, 660, L109
 Larsen, S. S., Brodie, J. P., Huchra, J. P., Forbes, D. A., & Grillmair, C. J. 2001, *AJ*, 121, 2974
 Lee, M. G., Hwang, H. S., Kim, S. C., Park, H. S., Geisler, D., Sarajedini, A., & Harris, W. E. 2008, *ApJ*, 674, 886
 Mei, S., Blakeslee, J. P., Côté, P., Tonry, J. L., West, M. J., Ferrarese, L., Jordán, A., Peng, E. W., Anthony, A., & Merritt, D. 2007, *ApJ*, 655, 144
 Menci, N., Rosati, P., Gobat, R., Strazzullo, V., Rettura, A., Mei, S., & Demarco, R. 2008, *ApJ*, 685, 863
 Mieske, S., et al. 2006, *ApJ*, 653, 193
 Mieske, S., et al. 2010, *ApJ*, in press
 Morgan, S., & Lake, G. 1989, *ApJ*, 339, 171
 Ngeow, C.-C., Kanbur, S. M., Neilson, H. R., Nanthakumar, A., & Buonaccorsi, J. 2009, *ApJ*, 693, 691
 Peng, E. W., et al. 2006, *ApJ*, 639, 95 (P06)
 Peng, E. W., et al. 2009, *ApJ*, 703, 42
 Puzia, T. H., Kissler-Patig, M., Thomas, D., Maraston, C., Saglia, R. P., Bender, R., Goudfrooij, P., & Hempel, M. 2005, *A&A*, 439, 997
 Puzia, T. H., Zepf, S. E., Kissler-Patig, M., Hilker, M., Minniti, D., & Goudfrooij, P. 2002, *A&A*, 391, 453
 Raimondo, G., Brocato, E., Cantiello, M., & Capaccioli, M. 2005, *AJ*, 130, 2625
 Recchi, S., & Danziger, I. J. 2005, *A&A*, 436, 145
 Renzini, A. 2006, *ARA&A*, 44, 141
 Spitler, L. R., Larsen, S. S., Strader, J., Brodie, J. P., Forbes, D. A., & Beasley, M. A. 2006, *AJ*, 132, 1593
 Spitler, L. R., Forbes, D. A., & Beasley, M. A. 2008, *MNRAS*, 389, 1150
 Strader, J., Beasley, M. A., & Brodie, J. P. 2007, *AJ*, 133, 2015
 Strader, J., Brodie, J. P., Spitler, L., & Beasley, M. A. 2006, *AJ*, 132, 2333
 Strader, J., & Smith, G. H. 2008, *AJ*, 136, 1828
 Thomas, D., Maraston, C., Bender, R., & Mendes de Oliveira, C. 2005, *ApJ*, 621, 673
 Toomre, A. 1977, *Evolution of Galaxies and Stellar Populations*, 401
 Wehner, E. M. H., Harris, W. E., Whitmore, B. C., Rothberg, B., & Woodley, K. A. 2008, *ApJ*, 681, 1233
 West, M., Cote, P., Peng, E., Jordán, A., Blakeslee, J., Takamiya, M., & Gregg, M. 2006, *NOAO Proposal ID #2006A-0114*, 114
 Yoon, S.-J., Yi, S. K., & Lee, Y.-W. 2006, *Science*, 311, 1129
 Yoon, S.-J. et al. 2010, submitted
 Zinn, R., & West, M. J. 1984, *ApJS*, 55, 45